Letter | Editors' Suggestion

Emergence of radial Rashba spin-orbit fields in twisted van der Waals heterostructures

Tobias Frank, Paulo E. Faria Junior,* Klaus Zollner, and Jaroslav Fabian
Institute for Theoretical Physics, University of Regensburg, 93040 Regensburg, Germany

(Received 19 February 2024; revised 22 May 2024; accepted 28 May 2024; published 12 June 2024)

Rashba spin-orbit coupling is a quintessential spin interaction appearing in virtually any electronic heterostructure. Its paradigmatic spin texture in the momentum space forms a tangential vector field. Using first-principles investigations, we demonstrate that in twisted homobilayers and heteromultilayers, the Rashba spin texture can be predominantly radial, parallel to the momentum. Specifically, we study four experimentally relevant structures: twisted bilayer graphene (Gr), twisted bilayer WSe_2, and twisted multilayers WSe_2/Gr/WSe_2 and WSe_2/Gr/Gr/WSe_2. We show that the Rashba spin texture in such structures can be controlled by an electric field, allowing to tune it from radial to tangential. Such spin-orbit engineering should be useful for designing spin-charge conversion and spin-orbit torque schemes, as well as for controlling correlated phases and superconductivity in van der Waals materials.

DOI: 10.1103/PhysRevB.109.L241403

Introduction. The Rashba effect is the appearance of an extrinsic spin-orbit coupling (SOC) at surfaces and interfaces of electronic materials. Following the study by Rashba and Sheka on wurtzite semiconductors [1], the effect was formulated by Bychkov and Rashba for 2D electron gas [2]; see the recent review [3]. The Rashba effect is at the heart of spintronics, allowing for efficient spin manipulation in a variety of spin transport, spin relaxation, and spin detection phenomena [4–8].

The advent of two-dimensional (2D) materials and van der Waals (vdW) heterostructures has significantly expanded the range of possibilities for controlling the electron spin [6–8]. In particular, novel spin interactions can be generated in vdW stacks by the proximity effect [9,10]. The prime example is the valley-Zeeman (Ising) SOC, induced in graphene (Gr) from a neighboring transition-metal dichalcogenide (TMDC) such as $MoSe_2$ or WSe_2, yielding a giant spin relaxation anisotropy [11–13] and with controllable spin precession by gate voltages in spin transistor devices at room temperature [14].

For Gr-based Dirac systems, in addition to the valley-Zeeman term, the breaking of space and mirror symmetries leads to the Rashba spin-orbit field (SOF). Pioneering tight-binding studies of twisted Gr/TMDC [15,16] proposed that the Rashba SOF in Gr acquires an "unconventional" radial component encoded in the so-called Rashba angle φ (between the electron's momentum and spin). The general form of this general Rashba coupling at K and K' points for $\mathcal{C}_3$ symmetric systems is

$$\mathcal{H}_{\mathrm{R}} = \lambda_{\mathrm{R}} e^{-i\varphi s_z/2}(\tau\sigma_x \otimes s_y + \sigma_y \otimes s_x)e^{i\varphi s_z/2}. \qquad (1)$$

The coupling constant λ_R denotes the strength of the Rashba SOF, $\tau = \pm 1$ is the valley index, σ_i are the pseudospin, and s_i spin Pauli matrices. If $\varphi = 0$, the Rashba field is tangential (conventional); if $\varphi = 90^\circ$, it is radial (unconventional). We note that the term "unconventional" has been previously used [17–21] to identify the spin-to-charge conversion along the direction of the applied electric field, also referred to as unconventional Rashba-Edelstein effect. This unconventional signature is directly linked to the radial component of the spin texture.

The Rashba angle φ has been calculated for twisted Gr/TMDC from first-principles [17,22–24] and by tight-binding modeling [25], as well as for Gr/1T-TaS_2 [26]. DFT calculations for twisted Gr/TMDCs [17,22,23] find that the Rashba angle varies between –20° and 40°, not being radial at any twist angle. Remarkably, the predicted variation of the Rashba angle has now been seen experimentally in Gr/WSe_2 bilayers [19], observing φ up to about $\pm 60^\circ$.

Here, we show that a radial Rashba SOF emerges in twisted homobilayers and multilayers of hexagonal lattices. Specifically, we perform first-principles calculations on four distinct structures: twisted bilayer graphene (TBLG), twisted bilayer WSe_2, twisted multilayers WSe_2/Gr/WSe_2, and WSe_2/TBLG/WSe_2. We show that in all the investigated cases the in-plane Rashba spin texture can be radial, $\varphi = 90^\circ$, but we also discuss cases in which it is not. For computational reasons, we use the twist angle of 21.8° (and the complementary 38.2°) for the homobilayers, noting that commensurate moiré crystals of bilayer WSe_2 twisted at these angles were recently demonstrated [27]. For such structures, our findings make even quantitative predictions. The origin of the radial Rashba SOF can be traced to the interference of two layer-locked (hidden in untwisted stacks) Rashba SOF that have opposite tangential, but the same radial components. Moreover, we demonstrate that the Rashba spin texture can be tuned from radial to tangential by a displacement ouf-of-plane electric field, particularly relevant to counteract undesired displacement fields that may be present in real devices.

Engineering the radial Rashba coupling would facilitate the unconventional charge-to-spin conversion in vdW heterostructures [17,18,20,21,23,28,29], improve the

*Contact author: fariajunior.pe@gmail.com

functionality of spin-orbit torque [30] by allowing the control the polarization of accumulated spin accumulation and spin current, and influence correlated phases [31–35], superconductivity [36–38], and magnetotransport [39]. Furthermore, a radial spin texture in a vdW heterostructure would emulate, in a controlled way, the 3D space group [40,41] predictions of the parallel spin-momentum locking in chiral materials such as tellurium [42,43] or chiral topological semimetals [44–46]. Very recently, chiral-induced spin selectivity has been predicted to be realized in vertical tunneling by twisted TMDCs [47]. Our first-principles calculations show that, while not being universal, the formation of a radial Rashba spin texture can be readily achieved in twisted vdW structures.

Moreover, with these radial spin textures we are bringing exciting manifestations of 3D group theory predictions [40,41] to the burgeoning field of 2D materials and their van der heterostructures.

Twisted bilayer graphene. Monolayer Gr exhibits an intrinsic spin-orbit splitting of tens of μeVs [48,49], and no Rashba coupling, while an out-of-plane electric field induces a Rashba splitting of about 10 μeV per each V/nm [48]. Similar values appear in bilayer graphene (BLG) [50,51].

The electronic structure of BLG with SOC can be described as comprising conventional layer-dependent Rashba SOF with opposite orientations in the two layers [50]; the net result is no overall Rashba field and no spin-orbit splitting of the bands. In effect, each layer exerts an effective electric field on the other layer, causing a Rashba coupling in it. This is similar to the concept of "hidden" spin polarization in inversion symmetric materials [52]. The application of an out-of-plane electric field induces layer polarization and removes the perfect balance of the hidden Rashba SOFs, giving a nonzero *conventional* Rashba spin texture [50]. Chirally stacked (ABC) graphene trilayers follow the same SOC trends [53,54].

How do the hidden, layer-dependent Rashba SOF manifest themselves in the electronic structure when the two layers get twisted? Without layer polarization, the two SOFs in the momentum space add up; if the fields of the hybridizing Bloch states from each layer are similar, these two tangential (but rotated) fields yield a purely radial, *unconventional* Rashba spin texture. Layer polarization—due to a out-of-plane electric field or the presence of a substrate—can add a tangential component and make the Rashba field fully in-plane tunable.

We illustrate this concept by performing first-principles simulations and effective modeling for 21.79° (sublattice-exchange) even and odd TBLG [55], which exhibit threefold rotational symmetry and resemble energy-renormalized versions of AA and AB (Bernal) BLG dispersions, respectively. The supercells are constructed following Shallcross *et al.* [56]. Further geometry setup details are given in [57]. Even TBLG has two overlapping atomic sites, see Fig. 1(b), whereas the odd structure has only one overlapping atomic site, see Fig. 1(c). In twisted structures, spatial modulation of the interlayer interaction provides momentum conservation for the coupling of different single-layer momentum states via Umklapp processes [55]. The interaction between the layers predominantly happens at the overlapping atomic sites and the reduction in the energy scale (with respect to BLG analogues) is a measure for the loss of interlayer registry [58].

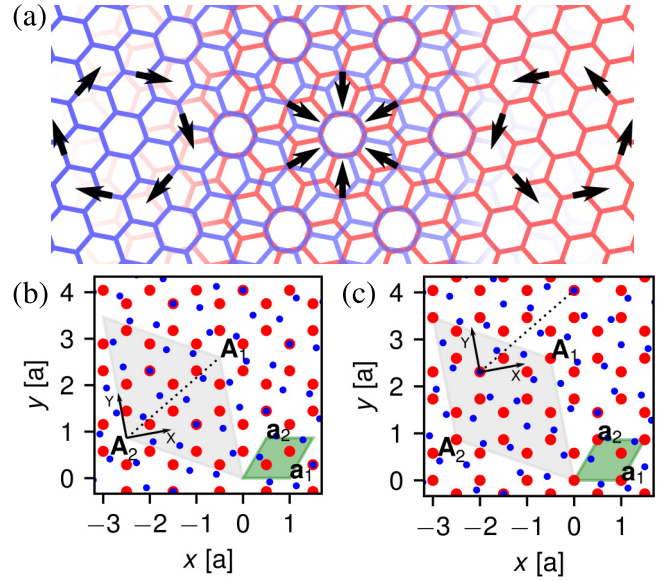

FIG. 1. (a) Sketch of radial Rashba emergence by the interference of oppositely rotating tangential Rashba fields. [(b),(c)] 21.79° TBLG ($p = 1, q = 3$) and different sublattice-exchange symmetries. The primitive cell of graphene with its lattice vectors $\mathbf{a}_{1/2}$ is indicated by the green rhombus. The shaded area is the moiré supercell with lattice vectors $\mathbf{A}_{1/2}$. The red/blue dots represent carbon atoms from the bottom/top layer. The even system (b) is obtained from AA stacking and rotation about the origin [0,0], the odd system (c) from initial AB (Bernal) stacking. The coordinate system for DFT calculations is shown by labels X and Y. In-plane twofold rotation axes are indicated by dashed lines.

The band structures of even and odd TBLGs are calculated by the `Wien2k` code [59], which accounts for *d* orbitals responsible for SOC in Gr [48] (for computational details see the Supplemental Material, SM [57]). The band structure and spin texture of the even system are shown in Fig. 2. We focus on the low-energy physics at the K point of the moiré lattice, indicated by the meV energy scale. The band structure exhibits two crossings at the K point, which are remnants of the Dirac cones of single-layer graphene separated in energy by 3.6 meV. Shifting the cones would resemble the rescaled AA-stacked BLG band structure [55,57]. However, the interlayer interaction opens a gap of 1.1 meV between the two copies of Dirac cones. The Dirac cones themselves are gapped (not visible) by a spin-orbit gap of 24 μeV as in single layer Gr [48]. The spin degeneracy is lifted by ∼10 μeV due to missing inversion symmetry. The spin texture of the highest valence band around K, shown in Fig. 2(b), form a purely radial Rashba SOF. All the low-energy bands have such a spin texture, with alternating directions pointing towards or away from the K point (see Sec. S2 of the SM [57] for all the calculated spin textures). Interestingly, the radial texture can be tuned to tangential by applying an out-of-plane electric field, as shown in Fig. 2(d) for the field of 29 mV/nm, while the band structure is hardly affected, see Fig. 2(c). This control of the spin texture using an out-of-plane electric field is crucial to counteract undesirable displacement fields that appear in real samples, thus improving the operation of spintronic devices.

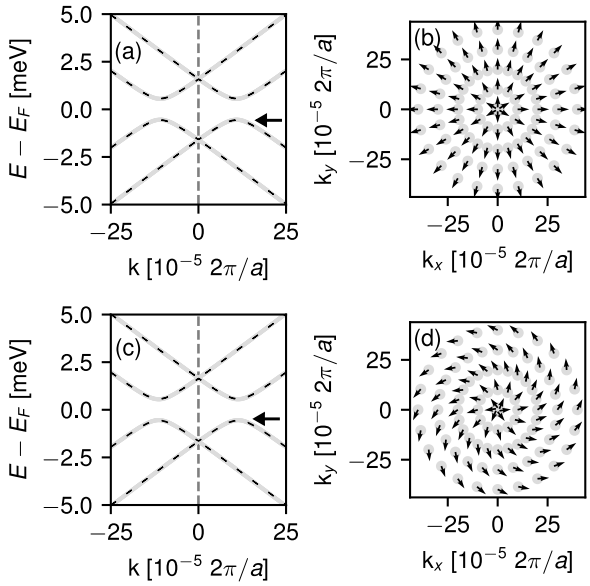

FIG. 2. *Ab initio* low-energy band structures and spin-fields of 21.79° *even* TBLG. (a) Low-energy TBLG band structure with corresponding (b) spin texture of the highest valence band, indicated by the horizontal arrow in (a). (c) TBLG band structure with an electric field 29 mV/nm with corresponding (d) spin texture of the highest valence band indicated by the horizontal arrow in (c). The spin texture encodes s_x and s_y components of the spin expectation value. The K point is marked by the vertical-dashed line. The color of the bands in (a) and (c) and the dots in (b) and (d) denote the spin-z expectation value, where red (blue) is spin-up (down) and grey color denotes zero polarization. In this particular system, the spin texture has only in-plane components therefore the energy bands in (a) and (c) as well as the dots in (b) and (d) appear with grey color. The dashed lines on top of the DFT bands are model fits with parameters $v_F = 8.16 \times 10^5$ m/s, $w = 1.597$ meV, $\lambda_I = -11.858$ μeV, $\lambda_R = 13.5$ μeV, and $u = 0.43$ meV.

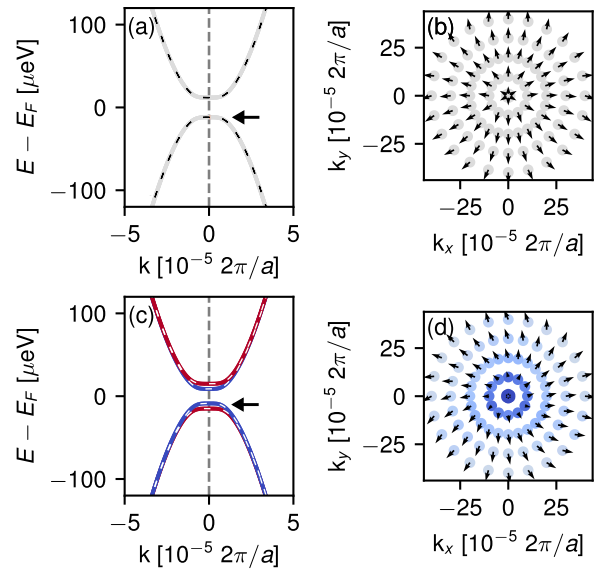

FIG. 3. Same as Fig. 2 but for 21.79°-rotated *odd* TBLG in an electric field of 29 μV/nm. Model fit parameters are $v_F = 8.16 \times 10^5$ m/s, $w = 1.685$ meV, $\phi = 0.171$, $\lambda_I = -11.858$ μeV, $\lambda_R = 0.3$ μeV, and $u = 3.1$ μeV.

In the case of the odd system, Fig. 3, the band structure has a quadratic dispersion, similar to AB-stacked BLG. The valence-conduction band degeneracy at K is lifted by the intrinsic spin-orbit gap of 23 μeV and band splittings on the sub-μeV scale are introduced. The parabolic second valence and conduction bands, see e.g., Ref. [55], are split off by 1.7 meV, outside the energy window. In the odd system we recognize a radial shape of the spin texture as well. The SOF shows some deviations from pure radial, because the symmetry is reduced from sixfold rotation to a threefold symmetry. Application of a tiny electric field of 29 μV/nm further opens the gap and the band splitting saturates at the intrinsic SOC energy scale. We find that the band structure becomes spin-polarized and that the spin texture acquires a tangential component.

In the SM [57] we present the band structure and spin textures for two additional cases: the twist angle 27.8°(sublattice even) and 32.2° (sublattice odd). Our calculations reveal that the predominant radial component in the spin texture also emerges for this set of twist angles, confirming the general nature of this phenomena. We also note that the emergence of the radial spin textures is consistent with the symmetry groups (with threefold or sixfold rotations) of the twisted structures predicted by group theory in 3D systems [40,41]. The calculated low-energy bands along with the spin textures can be quantitatively described by an effective model of TBLG with layer-dependent intrinsic and (hidden) Rashba couplings. We refer to [57] for details of the model, but present in Figs. 2 and 3 the fits.

We note that our calculated spin textures seem to be at odds with the recent report [60], which considered the same twist angle of TBLG, but found vortex-like spin textures at K, employing `VASP` code [61]. To crosscheck our results, we also employed `Quantum Espresso` [62] and confirmed the radial spin textures for both unrelaxed and relaxed geometries, without significant differences. Also, our effective model [57] fits well the DFT simulations, see Figs. 2 and 3, giving additional support for the emergence of radial Rashba fields. We found that the main difference is in the scale of the k space considered. In Sec. S2 of the SM [57] we present the spin texture for regions further away from the charge neutrality and found similar vortex-like spin textures as in Ref. [60], revealing that the trigonal character of the system is imprinted in the spin texture at some point.

Twisted WSe_2 *homobilayers.* To demonstrate that not only TBLG exhibits purely radial Rashba SOFs, we performed first-principles simulations of a twisted WSe_2 homobilayer using the `Wien2k` code [59]. Monolayer TMDCs such as WSe_2 lack space inversion symmetry, so their electronic states are naturally spin split. However, the presence of a horizontal mirror plane symmetry precludes the appearance of in-plane Rashba fields but rather enables robust spin polarization in the out-of-plane direction [63]. Conversely, naturally stacked bilayer TMDCs have space inversion symmetry and no spin-orbit polarization of their bands. The twisted structures start from a 0° stacking with W and Se atoms on top of each other (the R^h_h stacking [64,65], containing a horizontal mirror plane). We discuss here in the main text the commensurate

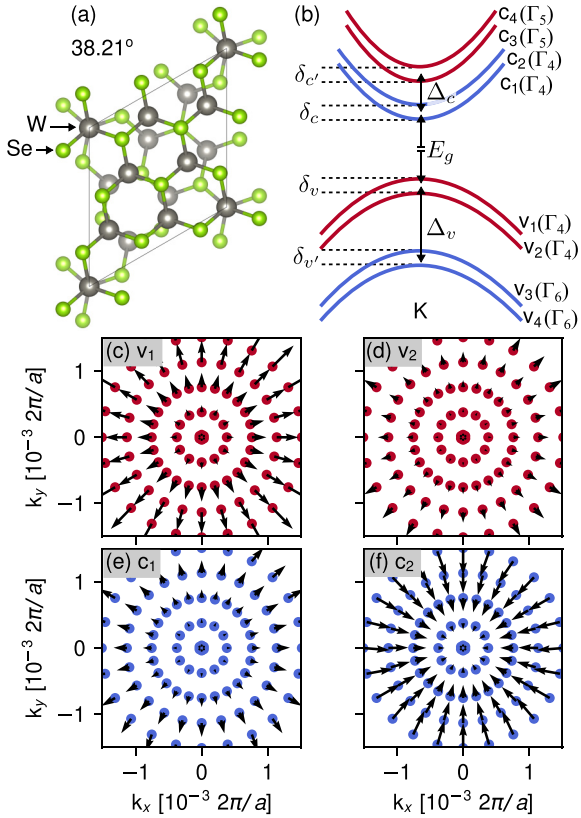

FIG. 4. Radial Rashba in twisted WSe_2 homobilayers. (a) 38.21° supercell with W and Se atoms indicated. (b) Sketch of the low-energy bands indicating the relevant energy splittings and their irreducible representations. The calculated *ab initio* splittings (in meV) are $E_g = 1352.79$, $\Delta_v = 453.22$, $\Delta_c = 40.65$, $\delta_{v'} = 4.29$, $\delta_v = 1.94$, $\delta_c = 0.63$, $\delta_{c'} = 0.24$. Calculated spin textures for the energy bands (c) v_1, (d) v_2, (e) c_1, and (f) c_2. The radial Rashba texture points outwards for v_1, v_2, and c_1 and inwards for c_2.

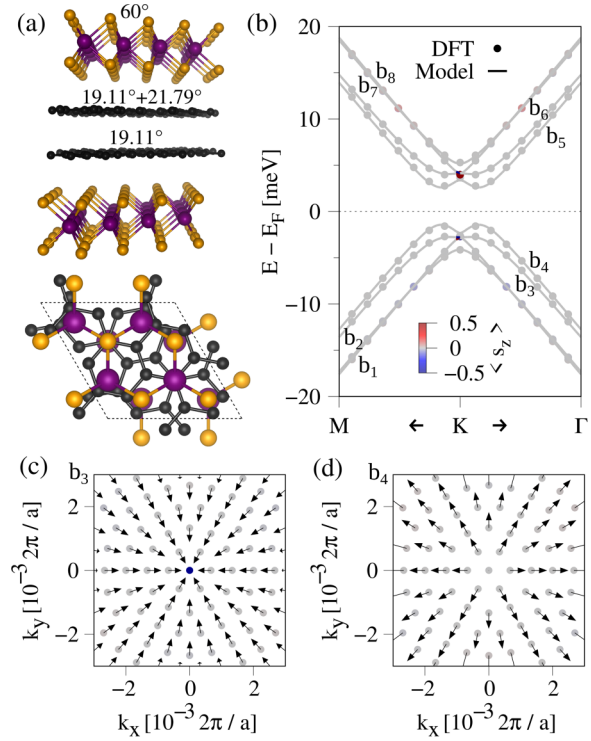

FIG. 5. Radial Rashba in WSe_2-encapsulated even TBLG. (a) Top and side view of the twisted multilayer stack. The twist angle indicated above each layer is measured with respect to the bottom WSe_2 layer. (b) The corresponding low-energy bands with a fit to the model Hamiltonian. (c) and (d) Exemplary spin textures of the bands b_3 and b_4 as labeled in (b).

unit cell for a twist angle of 38.21° with the corresponding atomic structure shown in Fig. 4(a). The symmetry groups of these structures are discussed in [57].

The band structure of the 38.21° supercell is presented in Fig. 4(b), indicating monolayer- and moiré-derived spin-orbit splittings, Δ (consistent with isolated monolayers [66]) and δ, respectively. The spin textures for the lowest energy bands, v_1-v_2 and c_1-c_2, are given in Figs. 4(c)–4(f). Despite the strong spin-valley locking (out-of-plane spins) [63], our calculations clearly reveal the emergence of in-plane radial Rashba textures in the vicinity of the K-valleys. The corresponding in-plane spin expectation values are on the order of $10^{-5} - 10^{-4}$, roughly three orders of magnitude smaller than in Gr systems (see Fig. S11 within the SM [57]) but well above the numerical precision [67]. In the SM [57], we show the full band structure and the spin textures for all the valence and conduction bands v_1-v_4 and c_1-c_4, as well as the same analysis for the complementary twist angle of 21.79°. Particularly, in the 21.79° case the radial Rashba spin textures acquire trigonal features that become more pronounced as we move away from the K valleys for particular energy bands, due to the hybridization of the Bloch states from different layers occurring at different points in the Brillouin zone. These distinct k points can exhibit hidden Rashba fields with unequal magnitudes and/or angular textures (see Fig. S7 within the SM [57] for monolayer WSe_2 under electric field).

WSe_2-encapsulated TBLG. BLG has weak Rashba coupling, but encapsulated by TMDCs the spin-splitting of BLG is on the meV scale, well within the reach of spin transport experiments. Here, we demonstrate the existence of unconventional Rashba coupling in twisted multilayer stacks, containing either monolayer Gr (see SM [57]) or TBLG, see Fig. 5. The twist angle of BLG is 21.79°, while the bottom layer of BLG is twisted by 19.11° from the adjacent WSe_2. To complete the chiral structure, the top WSe_2 monolayer is twisted by 60° with respect to the bottom WSe_2; see Fig. 5(a).

The energetically spin-split electronic states have no out-of-plane spin orientation, as shown in Fig. 5(b). The in-plane spin polarizations, presented in Figs. 5(c) and 5(d), are purely radial. The relative twist angle of the encapsulating WSe_2 layers allows to tailor the interference of layer-resolved Rashba and sublattice-odd valley-Zeeman couplings (see the SM [57]). The difference to BLG is the magnitude of the Rashba coupling, which is about 1 meV. We fit the DFT data to a model Hamiltonian in the SM [57]. The Hamiltonian description should be useful for investigating spin transport and correlation physics in such chiral multilayers. Importantly, the spin texture can turn from radial to tangential, upon applying an out-of-plane electric field (see the SM [57]).

Conclusions and outlook. We studied the emergence of purely radial SOFs in twisted homobilayers of Gr and WSe_2, as well as in twisted multilayer heterostructures comprising Gr and WSe_2. We found that this unconventional Rashba spin texture is fully in-plane tunable, from radial to tangential, by a displacement field. Such SOFs should be even more pronounced in homobilayers of strong spin-orbit materials with built-in Rashba SOC, such as Janus dichalcogenides [68] as well as in vdW heterostructures with strong interlayer coupling, which induces strong hidden Rashba fields.

The ramifications of our findings have direct impact in distinct research fields involving 2D materials and van der Waals heterostructures. For instance, it has been shown that the band topology of Gr can be modified by proximity effects [69–71] and that twisted (commensurate) bilayer Gr behaves as a topological crystalline insulator [72] with electric field tunable band gap [73]. These topological features can be explored in the context of correlation physics with proximity induced spin-orbit coupling [33,74], which strongly depend on the particular shapes of the spin textures of the underlying energy bands. Moreover, recent efforts in characterizing the orbital angular momentum of 3D chiral materials [75] also motivate future studies in the heterostructures we proposed, which will be particularly relevant to the emerging field of orbitronics in van der Waals systems.

Acknowledgments. The authors thank Martin Gmitra, Denis Kochan, Thomas Naimer, Tomasz Woźniak, and Niels Schröter for fruitful discussions. This work was funded by the Deutsche Forschungsgemeinschaft (DFG, German Research Foundation) SFB 1277 (Project ID 314695032) and SPP 2244 (Project No. 443416183). The authors gratefully acknowledge the Gauss Centre for Supercomputing (GCS) e.V. for funding this project by providing computing time on the GCS Supercomputer SuperMUC at Leibniz Supercomputing Centre.

[1] E. Rashba and V. Sheka, Symmetry of energy bands in crystals of wurtzite type: II. Symmetry of bands including spin-orbit interaction, Fiz. Tverd. Tela Collected Papers **2**, 62 (1959).
[2] Y. Bychkov and E. Rashba, Properties of a 2D electron gas with a lifted spectrum degeneracy, JETP Lett. **39**, 78 (1984).
[3] G. Bihlmayer, P. Noël, D. V. Vyalikh, E. V. Chulkov, and A. Manchon, Rashba-like physics in condensed matter, Nat. Rev. Phys. **4**, 642 (2022).
[4] I. Žutić, J. Fabian, and S. Das Sarma, Spintronics: Fundamentals and applications, Rev. Mod. Phys. **76**, 323 (2004).
[5] J. Fabian, A. Matos-Abiague, C. Ertler, P. Stano, and I. Žutić, Semiconductor spintronics, Acta Phys. Slovaca **57**, 565 (2007).
[6] W. Han, R. K. Kawakami, M. Gmitra, and J. Fabian, Graphene spintronics, Nat. Nanotechnol. **9**, 794 (2014).
[7] A. Avsar, H. Ochoa, F. Guinea, B. Özyilmaz, B. J. van Wees, and I. J. Vera-Marun, Colloquium: Spintronics in graphene and other two-dimensional materials, Rev. Mod. Phys. **92**, 021003 (2020).
[8] D. T. Perkins and A. Ferreira, Spintronics in 2D graphene-based van der Waals heterostructures, in *Encyclopedia of Condensed Matter Physics*, 2nd ed., edited by T. Chakraborty (Academic Press, Oxford, 2024), pp. 205–222.
[9] J. F. Sierra, J. Fabian, R. K. Kawakami, S. Roche, and S. O. Valenzuela, van der Waals heterostructures for spintronics and opto-spintronics, Nat. Nanotechnol. **16**, 856 (2021).
[10] I. Žutić, A. Matos-Abiague, B. Scharf, H. Dery, and K. Belashchenko, Proximitized materials, Mater. Today **22**, 85 (2019).
[11] A. W. Cummings, J. H. Garcia, J. Fabian, and S. Roche, Giant spin lifetime anisotropy in graphene induced by proximity effects, Phys. Rev. Lett. **119**, 206601 (2017).
[12] T. S. Ghiasi, J. Ingla-Aynés, A. A. Kaverzin, and B. J. Van Wees, Large proximity-induced spin lifetime anisotropy in transition-metal dichalcogenide/graphene heterostructures, Nano Lett. **17**, 7528 (2017).
[13] L. A. Benitez, J. F. Sierra, W. Savero Torres, A. Arrighi, F. Bonell, M. V. Costache, and S. O. Valenzuela, Strongly anisotropic spin relaxation in graphene-transition metal dichalcogenide heterostructures at room temperature, Nat. Phys. **14**, 303 (2018).
[14] J. Ingla-Aynés, F. Herling, J. Fabian, L. E. Hueso, and F. Casanova, Electrical control of valley-zeeman spin-orbit-coupling–induced spin precession at room temperature, Phys. Rev. Lett. **127**, 047202 (2021).
[15] Y. Li and M. Koshino, Twist-angle dependence of the proximity spin-orbit coupling in graphene on transition-metal dichalcogenides, Phys. Rev. B **99**, 075438 (2019).
[16] A. David, P. Rakyta, A. Kormányos, and G. Burkard, Induced spin-orbit coupling in twisted graphene-transition metal dichalcogenide heterobilayers: Twistronics meets spintronics, Phys. Rev. B **100**, 085412 (2019).
[17] S. Lee, D. J. P. de Sousa, Y.-K. Kwon, F. de Juan, Z. Chi, F. Casanova, and T. Low, Charge-to-spin conversion in twisted graphene/WSe_2 heterostructures, Phys. Rev. B **106**, 165420 (2022).
[18] A. Veneri, D. T. S. Perkins, C. G. Péterfalvi, and A. Ferreira, Twist angle controlled collinear Edelstein effect in van der Waals heterostructures, Phys. Rev. B **106**, L081406 (2022).
[19] H. Yang, B. Martín-García, J. Kimák, E. Schmoranzerová, E. Dolan, Z. Chi, M. Gobbi, P. Němec, L. E. Hueso, and F. Casanova, Twist-angle tunable spin texture in WSe_2/graphene van der Waals heterostructures, arXiv:2312.10227.
[20] N. Ontoso, C. K. Safeer, F. Herling, J. Ingla-Aynés, H. Yang, Z. Chi, B. Martin-Garcia, I. Robredo, M. G. Vergniory, F. de Juan, M. Reyes Calvo, L. E. Hueso, and F. Casanova, Unconventional charge-to-spin conversion in graphene/$MoTe_2$ van der Waals heterostructures, Phys. Rev. Appl. **19**, 014053 (2023).
[21] B. Zhao, B. Karpiak, D. Khokhriakov, A. Johansson, A. M. Hoque, X. Xu, Y. Jiang, I. Mertig, and S. P. Dash, Unconventional charge–spin conversion in Weyl-semimetal WTe2, Adv. Mater. **32**, 2000818 (2020).
[22] T. Naimer, K. Zollner, M. Gmitra, and J. Fabian, Twist-angle dependent proximity induced spin-orbit coupling in graphene/transition metal dichalcogenide heterostructures, Phys. Rev. B **104**, 195156 (2021).
[23] K. Zollner, S. M. João, B. K. Nikolić, and J. Fabian, Twist- and gate-tunable proximity spin-orbit coupling, spin relaxation anisotropy, and charge-to-spin conversion in heterostructures of graphene and transition metal dichalcogenides, Phys. Rev. B **108**, 235166 (2023).

[24] A. Pezo, Z. Zanolli, N. Wittemeier, P. Ordejón, A. Fazzio, S. Roche, and J. H. Garcia, Manipulation of spin transport in graphene/transition metal dichalcogenide heterobilayers upon twisting, 2D Mater. **9**, 015008 (2022).

[25] C. G. Péterfalvi, A. David, P. Rakyta, G. Burkard, and A. Kormányos, Quantum interference tuning of spin-orbit coupling in twisted van der Waals trilayers, Phys. Rev. Res. **4**, L022049 (2022).

[26] K. Szałowski, M. Milivojević, D. Kochan, and M. Gmitra, Spin–orbit and exchange proximity couplings in graphene/1T-TaS_2 heterostructure triggered by a charge density wave, 2D Mater. **10**, 025013 (2023).

[27] Y. Li, F. Zhang, V.-A. Ha, Y.-C. Lin, C. Dong, Q. Gao, Z. Liu, X. Liu, S. H. Ryu, H. Kim *et al.*, Tuning commensurability in twisted van der Waals bilayers, Nature (London) **625**, 494 (2024).

[28] J. Ingla-Aynés, I. Groen, F. Herling, N. Ontoso, C. K. Safeer, F. de Juan, L. E. Hueso, M. Gobbi, and F. Casanova, Omnidirectional spin-to-charge conversion in graphene/$NbSe_2$ van der Waals heterostructures, 2D Mater. **9**, 045001 (2022).

[29] C. K. Safeer, N. Ontoso, J. Ingla-Aynés, F. Herling, V. T. Pham, A. Kurzmann, K. Ensslin, A. Chuvilin, I. Robredo, M. G. Vergniory *et al.*, Large multidirectional spin-to-charge conversion in low-symmetry semimetal $MoTe_2$ at room temperature, Nano Lett. **19**, 8758 (2019).

[30] X. Han, X. Wang, C. Wan, G. Yu, and X. Lv, Spin-orbit torques: Materials, physics, and devices, Appl. Phys. Lett. **118**, 120502 (2021).

[31] J.-X. Lin, Y.-H. Zhang, E. Morissette, Z. Wang, S. Liu, D. Rhodes, K. Watanabe, T. Taniguchi, J. Hone, and J. I. A. Li, Spin-orbit–driven ferromagnetism at half moiré filling in magic-angle twisted bilayer graphene, Science **375**, 437 (2022).

[32] M. Xie and S. Das Sarma, Flavor symmetry breaking in spin-orbit coupled bilayer graphene, Phys. Rev. B **107**, L201119 (2023).

[33] Y. Zhumagulov, D. Kochan, and J. Fabian, Emergent correlated phases in rhombohedral trilayer graphene induced by proximity spin-orbit and exchange coupling, Phys. Rev. Lett. **132**, 186401 (2024).

[34] Y. Zhumagulov, D. Kochan, and J. Fabian, Swapping exchange and spin-orbit induced correlated phases in ex-so-tic van der Waals heterostructures, arXiv:2307.16025.

[35] J. M. Koh, J. Alicea, and E. Lantagne-Hurtubise, Correlated phases in spin-orbit-coupled rhombohedral trilayer graphene, Phys. Rev. B **109**, 035113 (2024).

[36] Y. Zhang, R. Polski, A. Thomson, E. Lantagne-Hurtubise, C. Lewandowski, H. Zhou, K. Watanabe, T. Taniguchi, J. Alicea, and S. Nadj-Perge, Enhanced superconductivity in spin-orbit proximitized bilayer graphene, Nature (London) **613**, 268 (2023).

[37] A. Jimeno-Pozo, H. Sainz-Cruz, T. Cea, P. A. Pantaleón, and F. Guinea, Superconductivity from electronic interactions and spin-orbit enhancement in bilayer and trilayer graphene, Phys. Rev. B **107**, L161106 (2023).

[38] L. Holleis, C. L. Patterson, Y. Zhang, H. M. Yoo, H. Zhou, T. Taniguchi, K. Watanabe, S. Nadj-Perge, and A. F. Young, Ising superconductivity and nematicity in Bernal bilayer graphene with strong spin-orbit coupling, arXiv:2303.00742.

[39] W.-H. Kang, M. Barth, A. Garcia-Ruiz, A. Mreńca-Kolasińska, M.-H. Liu, and D. Kochan, Magnetotransport signatures of the radial Rashba spin-orbit coupling in proximitized graphene, arXiv:2402.13424.

[40] C. Mera Acosta, L. Yuan, G. M. Dalpian, and A. Zunger, Different shapes of spin textures as a journey through the Brillouin zone, Phys. Rev. B **104**, 104408 (2021).

[41] D. Gosálbez-Martínez, A. Crepaldi, and O. V. Yazyev, Diversity of radial spin textures in chiral materials, Phys. Rev. B **108**, L201114 (2023).

[42] M. Sakano, M. Hirayama, T. Takahashi, S. Akebi, M. Nakayama, K. Kuroda, K. Taguchi, T. Yoshikawa, K. Miyamoto, T. Okuda, K. Ono, H. Kumigashira, T. Ideue, Y. Iwasa, N. Mitsuishi, K. Ishizaka, S. Shin, T. Miyake, S. Murakami, T. Sasagawa, and T. Kondo, Radial spin texture in elemental tellurium with chiral crystal structure, Phys. Rev. Lett. **124**, 136404 (2020).

[43] F. Calavalle, M. Suárez-Rodríguez, B. Martín-García, A. Johansson, D. C. Vaz, H. Yang, I. V. Maznichenko, S. Ostanin, A. Mateo-Alonso, A. Chuvilin, I. Mertig, M. Gobbi, F. Casanova, and L. E. Hueso, Gate-tuneable and chirality-dependent charge-to-spin conversion in tellurium nanowires, Nat. Mater. **21**, 526 (2022).

[44] B. Bradlyn, J. Cano, Z. Wang, M. G. Vergniory, C. Felser, R. J. Cava, and B. A. Bernevig, Beyond Dirac and Weyl fermions: Unconventional quasiparticles in conventional crystals, Science **353**, aaf5037 (2016).

[45] N. B. M. Schröter, D. Pei, M. G. Vergniory, Y. Sun, K. Manna, F. de Juan, J. A. Krieger, V. Süss, M. Schmidt, P. Dudin *et al.*, Chiral topological semimetal with multifold band crossings and long Fermi arcs, Nat. Phys. **15**, 759 (2019).

[46] J. A. Krieger, S. Stolz, I. Robredo, K. Manna, E. C. McFarlane, M. Date, B. Pal, J. Yang, E. B. Guedes, J. H. Dil *et al.*, Weyl spin-momentum locking in a chiral topological semimetal, Nat. Commun. **15**, 3720 (2024).

[47] G. Menichetti, L. Cavicchi, L. Lucchesi, F. Taddei, G. Iannaccone, P. Jarillo-Herrero, C. Felser, F. H. L. Koppens, and M. Polini, Giant chirality-induced spin polarization in twisted transition metal dichalcogenides, arXiv:2312.09169.

[48] M. Gmitra, S. Konschuh, C. Ertler, C. Ambrosch-Draxl, and J. Fabian, Band-structure topologies of graphene: Spin-orbit coupling effects from first principles, Phys. Rev. B **80**, 235431 (2009).

[49] J. Sichau, M. Prada, T. Anlauf, T. J. Lyon, B. Bosnjak, L. Tiemann, and R. H. Blick, Resonance microwave measurements of an intrinsic spin-orbit coupling gap in graphene: A possible indication of a topological state, Phys. Rev. Lett. **122**, 046403 (2019).

[50] S. Konschuh, M. Gmitra, D. Kochan, and J. Fabian, Theory of spin-orbit coupling in bilayer graphene, Phys. Rev. B **85**, 115423 (2012).

[51] L. Banszerus, B. Frohn, T. Fabian, S. Somanchi, A. Epping, M. Müller, D. Neumaier, K. Watanabe, T. Taniguchi, F. Libisch, B. Beschoten, F. Hassler, and C. Stampfer, Observation of the spin-orbit gap in bilayer graphene by one-dimensional ballistic transport, Phys. Rev. Lett. **124**, 177701 (2020).

[52] X. Zhang, Q. Liu, J.-W. Luo, A. J. Freeman, and A. Zunger, Hidden spin polarization in inversion-symmetric bulk crystals, Nat. Phys. **10**, 387 (2014).

[53] A. Kormányos and G. Burkard, Intrinsic and substrate induced spin-orbit interaction in chirally stacked trilayer graphene, Phys. Rev. B **87**, 045419 (2013).

[54] K. Zollner, M. Gmitra, and J. Fabian, Proximity spin-orbit and exchange coupling in ABA and ABC trilayer graphene van der Waals heterostructures, Phys. Rev. B **105**, 115126 (2022).

[55] E. J. Mele, Commensuration and interlayer coherence in twisted bilayer graphene, Phys. Rev. B **81**, 161405(R) (2010).

[56] S. Shallcross, S. Sharma, and O. Pankratov, Emergent momentum scale, localization, and van Hove singularities in the graphene twist bilayer, Phys. Rev. B **87**, 245403 (2013).

[57] See Supplemental Material at http://link.aps.org/supplemental/10.1103/PhysRevB.109.L241403 for the computational details on the first principles calculations, the effective Hamiltonians for TBLG cases and further information on the twisted WSe_2 homobilayers and the twisted multilayers (WSe_2/graphene/WSe_2) and (WSe_2/graphene)/(graphene/WSe_2). It also contains Refs. [17,22,23,48,50,55,56,59,62,76–93].

[58] E. J. Mele, Band symmetries and singularities in twisted multilayer graphene, Phys. Rev. B **84**, 235439 (2011).

[59] P. Blaha, K. Schwarz, F. Tran, R. Laskowski, G. K. Madsen, and L. D. Marks, WIEN2k: An APW+lo program for calculating the properties of solids, J. Chem. Phys. **152**, 074101 (2020).

[60] K. Yananose, G. Cantele, P. Lucignano, S.-W. Cheong, J. Yu, and A. Stroppa, Chirality-induced spin texture switching in twisted bilayer graphene, Phys. Rev. B **104**, 075407 (2021).

[61] G. Kresse and J. Furthmüller, Efficient iterative schemes for *ab initio* total-energy calculations using a plane-wave basis set, Phys. Rev. B **54**, 11169 (1996).

[62] P. Giannozzi, S. Baroni, N. Bonini, M. Calandra, R. Car, C. Cavazzoni, D. Ceresoli, G. L. Chiarotti, M. Cococcioni, I. Dabo *et al.*, QUANTUM ESPRESSO: a modular and open-source software project for quantum simulations of materials, J. Phys.: Condens. Matter **21**, 395502 (2009).

[63] D. Xiao, G.-B. Liu, W. Feng, X. Xu, and W. Yao, Coupled spin and valley physics in monolayers of MoS_2 and other group-VI dichalcogenides, Phys. Rev. Lett. **108**, 196802 (2012).

[64] K. Tran, G. Moody, F. Wu, X. Lu, J. Choi, K. Kim, A. Rai, D. A. Sanchez, J. Quan, A. Singh *et al.*, Evidence for moiré excitons in van der Waals heterostructures, Nature (London) **567**, 71 (2019).

[65] P. E. Faria Junior and J. Fabian, Signatures of electric field and layer separation effects on the spin-valley physics of $MoSe_2$/WSe_2 heterobilayers: From energy bands to dipolar excitons, Nanomaterials **13**, 1187 (2023).

[66] A. Kormányos, G. Burkard, M. Gmitra, J. Fabian, V. Zólyomi, N. D. Drummond, and V. Fal'ko, $\mathbf{k}\cdot\mathbf{p}$ theory for two-dimensional transition metal dichalcogenide semiconductors, 2D Mater. **2**, 022001 (2015).

[67] M. Kurpas, P. E. Faria Junior, M. Gmitra, and J. Fabian, Spin-orbit coupling in elemental two-dimensional materials, Phys. Rev. B **100**, 125422 (2019).

[68] D. Soriano and J. L. Lado, Spin–orbit correlations and exchange-bias control in twisted Janus dichalcogenide multilayers, New J. Phys. **23**, 073038 (2021).

[69] M. Gmitra, D. Kochan, P. Högl, and J. Fabian, Trivial and inverted Dirac bands and the emergence of quantum spin Hall states in graphene on transition-metal dichalcogenides, Phys. Rev. B **93**, 155104 (2016).

[70] T. Frank, P. Högl, M. Gmitra, D. Kochan, and J. Fabian, Protected pseudohelical edge states in $\mathbb{Z}_2$-trivial proximitized graphene, Phys. Rev. Lett. **120**, 156402 (2018).

[71] P. Högl, T. Frank, K. Zollner, D. Kochan, M. Gmitra, and J. Fabian, Quantum anomalous Hall effects in graphene from proximity-induced uniform and staggered spin-orbit and exchange coupling, Phys. Rev. Lett. **124**, 136403 (2020).

[72] M. Kindermann, Topological crystalline insulator phase in graphene multilayers, Phys. Rev. Lett. **114**, 226802 (2015).

[73] S. Talkington and E. J. Mele, Electric-field-tunable band gap in commensurate twisted bilayer graphene, Phys. Rev. B **107**, L041408 (2023).

[74] T. Wang, M. Vila, M. P. Zaletel, and S. Chatterjee, Electrical control of spin and valley in spin-orbit coupled graphene multilayers, Phys. Rev. Lett. **132**, 116504 (2024).

[75] Y. Yen, J. A. Krieger, M. Yao, I. Robredo, K. Manna, Q. Yang, E. C. McFarlane, C. Shekhar, H. Borrmann, S. Stolz *et al.*, Controllable orbital angular momentum monopoles in chiral topological semimetals, arXiv:2311.13217.

[76] S. Grimme, J. Antony, S. Ehrlich, and H. Krieg, A consistent and accurate *ab initio* parametrization of density functional dispersion correction (DFT-D) for the 94 elements H-Pu, J. Comput. Chem. **132**, 154104 (2010).

[77] E. Mostaani, N. D. Drummond, and V. I. Fal'ko, Quantum Monte Carlo calculation of the binding energy of bilayer graphene, Phys. Rev. Lett. **115**, 115501 (2015).

[78] D. Weckbecker, S. Shallcross, M. Fleischmann, N. Ray, S. Sharma, and O. Pankratov, Low-energy theory for the graphene twist bilayer, Phys. Rev. B **93**, 035452 (2016).

[79] R. Bistritzer and A. H. MacDonald, Moiré bands in twisted double-layer graphene, Proc. Natl. Acad. Sci. USA **108**, 12233 (2011).

[80] D. Kochan, S. Irmer, and J. Fabian, Model spin-orbit coupling Hamiltonians for graphene systems, Phys. Rev. B **95**, 165415 (2017).

[81] J. P. Perdew, K. Burke, and M. Ernzerhof, Generalized gradient approximation made simple, Phys. Rev. Lett. **77**, 3865 (1996).

[82] D. J. Singh and L. Nordstrom, *Planewaves, Pseudopotentials, and the LAPW Method* (Springer Science & Business Media, 2006).

[83] P. E. Faria Junior, K. Zollner, T. Woźniak, M. Kurpas, M. Gmitra, and J. Fabian, First-principles insights into the spin-valley physics of strained transition metal dichalcogenides monolayers, New J. Phys. **24**, 083004 (2022).

[84] K.-Q. Lin, P. E. Faria Junior, J. M. Bauer, B. Peng, B. Monserrat, M. Gmitra, J. Fabian, S. Bange, and J. M. Lupton, Twist-angle engineering of excitonic quantum interference and optical nonlinearities in stacked 2D semiconductors, Nat. Commun. **12**, 1553 (2021).

[85] K. Uchida, S. Furuya, J.-I. Iwata, and A. Oshiyama, Atomic corrugation and electron localization due to moiré patterns in twisted bilayer graphenes, Phys. Rev. B **90**, 155451 (2014).

[86] S. R. Bahn and K. W. Jacobsen, An object-oriented scripting interface to a legacy electronic structure code, Comput. Sci. Eng. **4**, 56 (2002).

[87] P. Lazic, Cellmatch: Combining two unit cells into a common supercell with minimal strain, Comput. Phys. Commun. **197**, 324 (2015).

[88] D. S. Koda, F. Bechstedt, M. Marques, and L. K. Teles, Coincidence lattices of 2D crystals: Heterostructure predictions and applications, J. Phys. Chem. C **120**, 10895 (2016).

[89] S. Carr, S. Fang, and E. Kaxiras, Electronic-structure methods for twisted moiré layers, Nat. Rev. Mater. **5**, 748 (2020).

[90] G. Kresse and D. Joubert, From ultrasoft pseudopotentials to the projector augmented-wave method, Phys. Rev. B **59**, 1758 (1999).

[91] S. Grimme, Semiempirical GGA-type density functional constructed with a long-range dispersion correction, J. Comput. Chem. **27**, 1787 (2006).

[92] V. Barone, M. Casarin, D. Forrer, M. Pavone, M. Sambi, and A. Vittadini, Role and effective treatment of dispersive forces in materials: Polyethylene and graphite crystals as test cases, J. Comput. Chem. **30**, 934 (2009).

[93] L. Bengtsson, Dipole correction for surface supercell calculations, Phys. Rev. B **59**, 12301 (1999).